AIMS Materials Science, 4(2): 522-539.
DOI: 10.3934/matersci.2017.2.522
Received: 30 December 2016
Accepted: 28 March 2017
Published: 05 April 2017

http://www.aimspress.com/journal/Materials

*Research article*

# Surface-enhanced Raman spectroscopy detection of protein-ligand binding using D-glucose and glucose binding protein on nanostructured plasmonic substrates

**Luis Gutierrez-Rivera [1,2], Robert Peters [1,2], Steven Dew [1,2], and Maria Stepanova [1,2,*]**

[1] Department of Electrical and Computer Engineering, University of Alberta, 9211-116 Street NW, Edmonton, AB, T6G 1H9, Canada
[2] National Institute for Nanotechnolgy NRC, 11421 Saskatchewan Drive, Edmonton, AB, T6G 2M9, Canada

* **Correspondence:** Email: ms1@ualberta.ca.

**Abstract:** Conjugated nano-biological architectures interfacing solid nano-structured surfaces with biological polymers have gained significant attention due to their potential biosensing and biocatalytic applications. However, efficient characterization of such integrated systems remains a challenge. We describe surface enhanced Raman spectroscopy (SERS) detection of complex of D-glucose with glucose binding protein (GBP) immobilized on substrates. Substrates comprised of dense Ag nanostructure arrays on Ni-coated fused silica wafers were fabricated employing ultrahigh resolution electron beam lithography. Glucose-bound and glucose-free histidine-tagged GBP was immobilized on the substrates and probed using SERS while the samples were kept in solution, and the observed Raman spectra were recorded. Three substrate designs were tested for SERS detection of the protein-ligand binding. SERS spectra of immobilized glucose-free and glucose-bound GBP exhibited pronounced differences in their Raman signatures, demonstrating the potential of SERS as a sensitive method for the detection of protein-ligand molecular recognition on a solid surface. However, morphology of the nano-patterned plasmonic structures was found to influence the SERS signatures significantly. In order to interpret the findings, simulations of electric field around the nano-structured substrates were performed. An interplay of two factors, the availability of space between Ag features where the GBP could bind to Ni, and the effectiveness of the electromagnetic enhancement of the Raman scattering in “hot spots” between these features, was concluded to determine the observed trends.

**Keywords:** bio-functionalized nanostructured surfaces; molecular recognition; nanolithography; plasmonic nanostructures; surface-enhanced Raman spectroscopy; experiment and modeling

## 1. Introduction

Integrated nano-biological systems interfacing solid nanostructures with biological polymers are expected to revolutionize bio-sensing and bio-actuation technologies in the near future. Next-generation bio-electronic devices, drug delivery and bio-diagnostic systems are just a few examples of applications of integrated nano-biological architectures [1,2,3]. In order to enable rational design of such integrated systems, appropriate detection methods are required that will allow identification and characterization of biological polymers confined on surfaces of nano-electronic devices. In particular, surface enhanced Raman spectroscopy (SERS) has emerged as a highly promising technique for biosensing [4,5,6]. SERS allows for the detection of unique signatures corresponding to molecular vibrations, which identify the molecules absorbed on metallic nano-structured surfaces. The excitation of localized surface plasmons by light interacting with Au or Ag nanostructures increases dramatically the intensity of Raman scattering of light by the analyte adsorbed on or near the nanostructures, making SERS a unique technique for detecting various analytes including biological polymers and small molecules [4–7].

One of the challenges for SERS biosensing, however, is that the creation of electromagnetic "hot spots" (localized regions where the Raman scattering is substantially enhanced) requires metallic structures patterned at the deep nanoscale. Due to the sensitivity of SERS to small feature variations, such structures also need to be uniform and reproducible [6]. A variety of fabrication methods have been reported to produce SERS substrates [6–11]. In particular, electron beam lithography (EBL) [12,13] offers superb control over features down to below 10 nm, and also flexibility to allow for various designs. Despite the complexities of EBL, the high level of control over shape and position of nanostructures that it offers makes it one of the most promising techniques for SERS substrate fabrication [6–11]. In our earlier works [14,15,16], we have optimized EBL-based processes to fabricate dense arrays of noble metal nanostructures on dielectric substrates as required for efficient localization of plasmonic waves, and demonstrated SERS biodetection [16,17]. However, much remains to be done to allow for a rational selection of SERS substrates for optimal detection of specific analytes. Although it is clear that the substrate's geometry details such as the width of gaps between metal features play a crucial role [16,17], in-depth analysis of the substrate dependence is required for various analytes.

In this work, we investigate the influence of various substrate geometries on SERS spectra of immobilized glucose binding protein (GBP) both in apo-form and bound with its specific ligand, D-glucose. Although SERS detection of glucose and related compounds has been reported previously [18,19,20], surface chemistry that would enable an efficient adsorption remains a challenge. Recently, we have demonstrated [17] that surface-immobilized GBP may be employed as a specific recognition element for SERS detection of glucose. However, the GBP that we employed as a recognition element belongs to the periplasmic ligand binding (PLB) superfamily of proteins [21] which undergo hinge-bending conformational changes upon binding with their respective ligands. Although these conformational changes *per se* may be detected, and as such they make PLB proteins potentially very useful recognition elements for biosensors [22,23] they also add a dimension of

complexity into the interpretation of SERS data. Here, we explore the influence of substrate geometry on the observed SERS bands of glucose-free and glucose-bound GBP immobilized on nanostructured substrates with three different morphologies. In order to interpret observed differences in SERS signal intensities, simulations of the electric field were performed and experimental results discussed in the context of the numerical predictions.

## 2. Materials and Methods

### *2.1. Fabrication of Ag Nanostructures*

SERS substrates fabricated in this work involved Ag nanostructures on Ni-coated fused silica (FS) wafers. In this design, Ag nanostructures were used as an effective plasmonic media [4–11] requiring a high degree of localization of the plasmonic waves [23] on the insulating FS substrates. Ni coating was required to bind the hisidine-tagged GPB recognition element to the substrate [23].

Arrays of Ag nanostructures on fused silica substrates were fabricated using the EBL-based process illustrated in Figure 1. The FS wafers were cleaned in piranha ($H_2SO_4$:$H_2O_2$) solution; then a 10 nm layer of nickel was evaporated on the FS substrate using a JUV E-Gun Evaporator system. Next, polymethylmethacrylate (PMMA) 950K A2 resist was spin-coated on the Ni film to provide an approximately 90 nm thick layer. Then the samples were baked on a hotplate at 180 °C for 5 min. A 70 nm thick anti-charging layer of aquaSAVE (Mitsubishi Rayon Co.) water-soluble conductive polymer was subsequently spin-coated onto the PMMA following procedures described elsewhere [14–17]. Next, electron beam lithography was performed to generate arrays of nano-patterns in PMMA employing a Raith $150^{TWO}$ instrument. EBL exposures were done using 30 keV accelerating voltage, a 7.5 μm aperture and 23 pA electron beam current. The exposed patterns comprised two designs: periodic arrays of single-pixel dots with a 40 nm pitch, and periodic arrays of hexagon structures with side length of 100 nm. The average area exposure doses of 105 μC/cm$^2$ and 170 μC/cm$^2$, respectively, were found to result in high quality nanopatterns [17]. The exposed samples were developed in a 7:3 mixture of isopropyl alcohol (IPA) and deionized water (DI water) at room temperature. As a result, arrays of nano-pits and honeycomb-like structures with inter-feature distances of about 25 nm were fabricated in PMMA.

The nano-patterned PMMA layers were used as lift-off masks to fabricate Ag nanostructures on the substrates. This was achieved using electron beam evaporation of Ag with a customized Kurt J. Lesker water-cooled bell jar electron beam evaporation system, which provided a 10 nm thick silver film. Due to its thinness and relatively poor wetting, this film is discontinuous. After evaporation, a lift-off process was used to remove the PMMA mask from the substrate and obtain arrays of silver dots or hexagon-like structures on the Ni-coated FS substrates. Sonication in acetone for 15 seconds was performed to remove the resist. The area of the resulting Ag nano-arrays was approximately 10 μm × 4 μm. In order to monitor the quality of the SERS substrates fabricated, the substrates were imaged with a Hitachi S-4800 scanning electron microscope (SEM). Figures 2(a) and 2(b) show SEM imaged examples of arrays of Ag nano-dots and nano-hexagons, respectively, with approximately 25 nm wide inter-feature gaps on a Ni-coated FS wafer. In addition, we also fabricated plain Ag pad substrates as shown in Figure 2(c) for comparison. Such substrates were composed of Ni-coated FS wafers with a uniform 10 nm thick Ag layer evaporated over the Ni film.

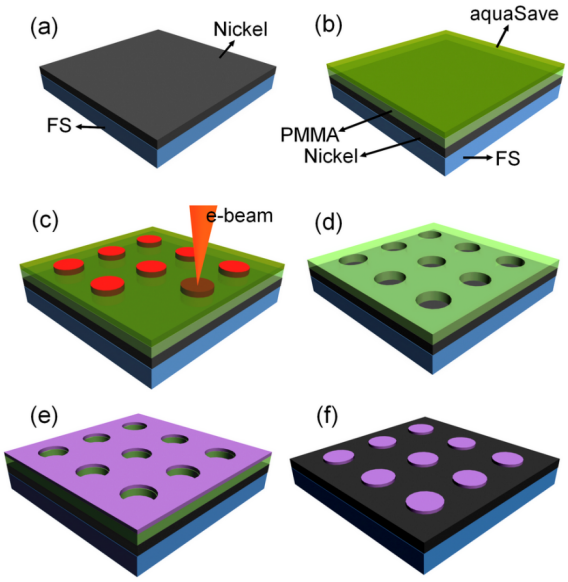


**Figure 1.** Schematic of the electron beam lithography (EBL) fabrication process for the SERS substrates Ag-Ni-FS [14,15,16]: (a) nickel evaporation on fused silica substrate; (b) polymethylmetacrylate (PMMA) and aquaSAVE spin-coating; (c) EBL exposure; (d) nanopits in the PMMA after development; (e) silver evaporation, and (f) silver nano-dots on Ni-coated FS after lift-off.

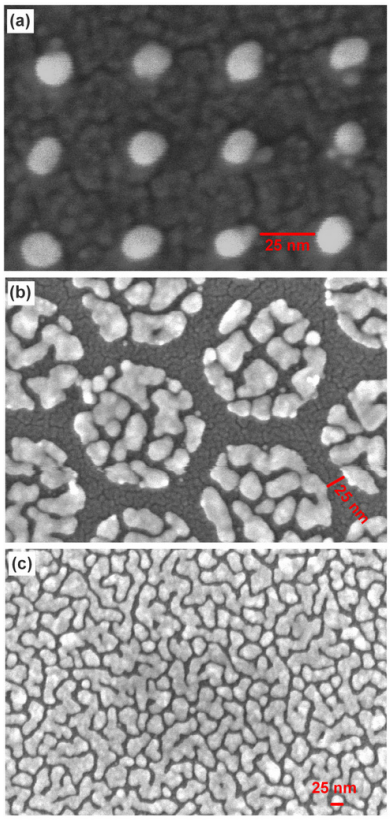


**Figure 2.** SEM images of Ag nanostructures of 10 nm thickness formed on Ni-coated FS: (a) Ag nano-dots; (b) Ag nano-hexagons; (c) Ag pad [17].

*2.2. Immobilization of Glucose Binding Protein on SERS Substrates*

A 0.9 mM solution of recombinant histidine-tagged glucose binding protein [25,26] in potassium phosphate buffer ($K_2HPO_4$, 25 mM, pH = 7.5) was prepared. The solution was used to further prepare two sets of samples for SERS measurements: one set with ligand-free GBP and another with ligand-bound protein. For ligand-free samples, a drop of GBP solution was deposited on the SERS substrates which were then incubated at 5 °C for 24 h. Then, the samples were rinsed with potassium phosphate buffer three times at room temperature without drying. To prepare ligand-bound samples, 30 µl of D-glucose (ligand) in buffer solution with a concentration of 100 mM were added to 30 µl of the GBP 0.9 mM solution using a plastic microtube container of 1 ml and a micropipette. A 30 min incubation at room temperature was used to allow for the binding process between GBP and D-glucose to occur. Then, 20 µl of the mixture was deposited on the SERS substrates. The samples were stored at 5 °C for 24 h to permit the immobilization of the ligand-bound protein. Coordination of nickel ions at the surface of the Ni coating by nitrogen-containing groups of histidine affinity tags [23] is known to allow for efficient chemisorption of tagged proteins. Moreover, by connecting GBP's termini to the surface of Ni coating, histidine tags are expected to ensure a relatively uniform orientation of surface-bound GBP, as schematically illustrated in Figure 3. After the incubation, the samples were rinsed with the buffer three times. Further details of the immobilization process and sample preparation can be found elsewhere [17]. The SERS substrates with immobilized ligand-free and ligand-bound GBP were subsequently characterized by Raman spectroscopy as described below. Due to a propensity of silver nanostructures to oxidation, each substrate was utilized once without reuse.

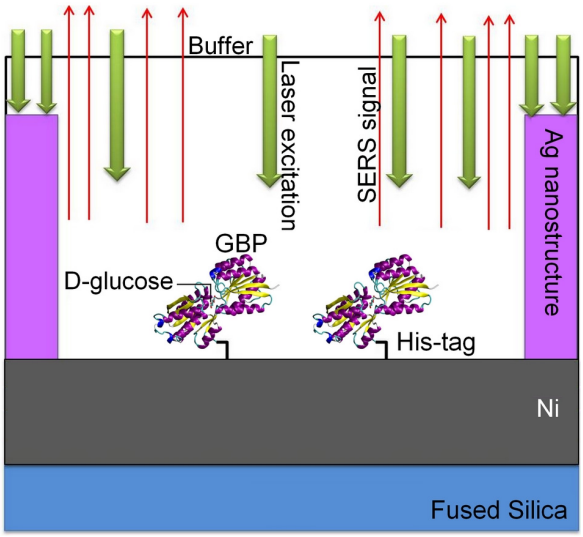


**Figure 3.** Scheme for protein-ligand complex detection using SERS. The structure of histidine-tagged (his-tag) GBP with D-glucose in ligand-binding pocket shown in the figure was taken from Protein Data Bank, PDB ID 2HPH [25].

*2.3. Raman Spectroscopy*

A Nicolet Almega XR instrument was used for collecting Raman spectra, employing 2.5 mW

laser power and 532 nm excitation wavelength. For an objective lens of 50×, the diameter for the laser spot size was approximately 0.7 μm. To avoid degradation of GBP due to exposure to laser light, short acquisition time of 5 sec. per sample was used [17]. To validate reproducibility, multiple SERS spectra were obtained on three separately prepared substrates, with five spots used in the area of the sample containing Ag nanostructures. There was a high degree of qualitative and detailed consistency between spectra taken under comparable experimental conditions.

Our SERS characterization of substrate-immobilized protein with and without ligand is illustrated by Figure 3. During the detection, the samples were immersed in potassium phosphate buffer. Bio-functionalized 1 cm × 1 cm diced substrates with the buffer deposited on their surfaces were placed on a microscope slide. To avoid evaporation of the buffer solution by laser exposure during the Raman spectroscopy, the samples were enclosed in a specially designed liquid-proof chamber covered by a microscope slide of 200 μm thickness [17]. For benchmarking purposes, we also obtained Raman spectra from buffer solutions of both apo-GBP and D-glucose with varying concentrations.

### *2.4. Field Simulations*

SERS signal enhancement depends on the excitation of localized electromagnetic waves (localized surface plasmons) producing very high electromagnetic fields around metallic nano-structures [27,28]. In order to better understand such processes, finite-element modeling in the framework of classical electromagnetic theory has proven to be very efficient [29–32]. We have calculated the fields around the Ag nanostructures employing the RF module from COMSOL Multiphysics 4.3 software [33]. We have performed calculations for arrays of Ag nano-dots and hexagons similar to those pictured in the SEM images as seen in Figures 2(a) and 2(b), respectively, and simulated the electromagnetic field around these nanostructures exposed to an excitation wavelength of 532 nm. The complex diffractive index of silver taken from experimental data [34] was used to calculate the relative permittivity of Ag as a function of the excitation wavelength. To simplify the calculations, our model assumes that the Ag nanostructures are located directly on a dielectric FS substrate without the Ni layer. Such a model predicts the strongest possible level of the field for a given Ag nanostructure. The model considers an incident wave propagating perpendicular to the surface of the substrate (xy plane). As plasmons can only be excited when the electric field (axis y) is in the plane of incidence (yz plane), polarized light is considered. With the wavevector **K** directed opposite to the z-axis, the electric field lies in the plane of incidence which is considered to be the yz plane. Then the incident electric field is $E_y = E_0 \cdot e^{2\pi i/\lambda z}$, where the constant $E_0$ is related to the laser power used to produce an excitation wavelength ($\lambda$). Here, $E_0 = 1 \times 10^8$ (V/m) and $\lambda = 532$ nm. A hollow spherical shell was used to determine the boundary conditions with perfectly matched layers (PML) on the system. The PMLs match the optical index at the interface and attenuate travelling waves exponentially to prevent artifact back-reflected waves from the outer boundaries [35].

## 3. Results

For benchmarking purposes, we first obtained Raman spectra from buffer solutions of GBP and of ligand (D-glucose) without structured substrates. The corresponding spectra for the GPB solution

with three different concentrations, 0.3, 0.9 and 1.3 mM, are shown in Figure 4(a). In the figure, the broad band around 3300–3500 $cm^{-1}$ corresponds to vibrations of O–H bonds in the buffer solution, whereas the band at 2935 $cm^{-1}$ likely represents vibrations involving C–H bonds of the protein [36–39]. It can be seen that the latter becomes more pronounced when the protein concentration increases. Figure 4(b) shows the Raman spectrum for D-glucose (ligand) in buffer solution for different concentrations of 1, 6, 100, 200, and 400 mM. In the case of the ligand, when the concentration is increased, C–H Raman bands arise at 2890 $cm^{-1}$ and 2960 $cm^{-1}$, and a less pronounced band can be discerned at 1130 $cm^{-1}$.

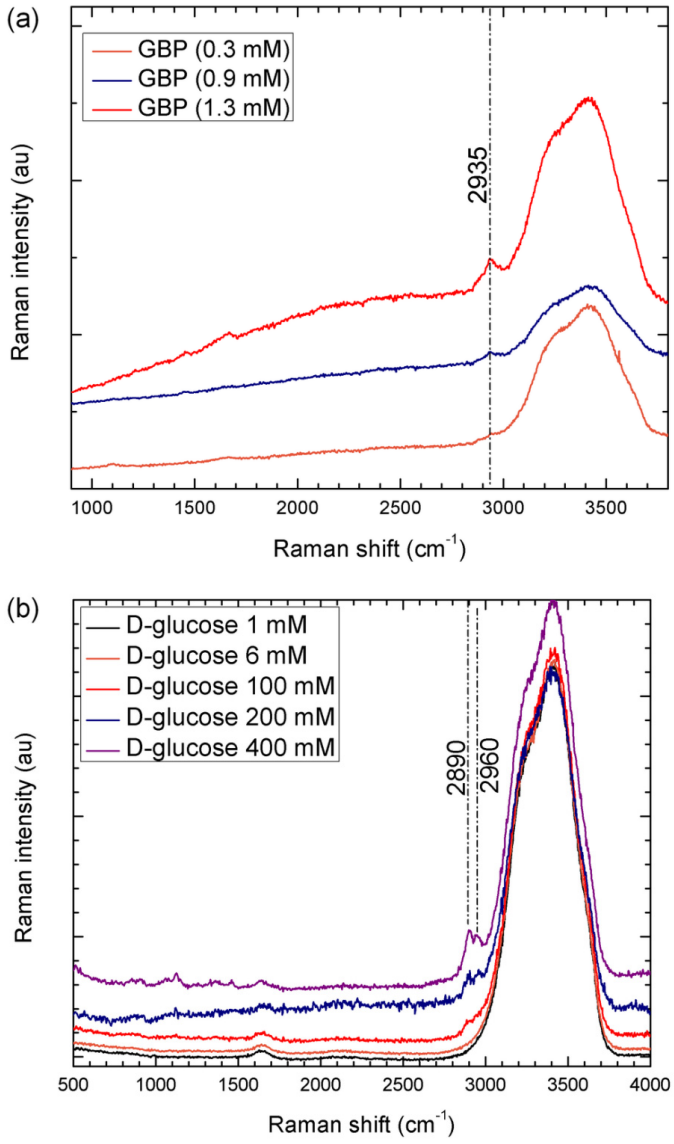


**Figure 4.** Raman spectra for solutions with different concentrations of glucose binding protein (a) and D-glucose ligand (b) in potassium phosphate buffer, for an excitation wavelength 532 nm [17].

Ligand-free and ligand-bound histidine-tagged glucose binding protein were immobilized on SERS substrates composed of Ag nanostructures on Ni-covered FS wafers as described in Section 2.

Ag nanostructures were used as a plasmonic media; an underlying FS wafer was required for localization of the plasmonic waves; and a Ni coating was needed to facilitate the binding of histidine-tagged proteins to the substrate. During the SERS detection, the samples were immersed in the potassium phosphate buffer to maintain the proteins in a fluid environment. Figure 5 shows the SERS spectra of ligand-free GBP immobilized on the three substrates shown in Figures 2(a), 2(b), and 2(c). All spectra in Figure 5 exhibit a broad band around 3300–3500 $cm^{-1}$, which corresponds to potassium phosphate buffer solution. The spectra obtained with Ag nano-dots (see Figure 2(a) and green line in Figure 5) and nano-hexagons (Figure 2(b) and red line in Figure 5) show a broad band centered around 1550 $cm^{-1}$ that originates from various vibrations in the immobilized protein [36–39]. A narrower band around 2933 $cm^{-1}$ is similar to that observed in Figure 4(a) and corresponds to C–H vibrations also generated by the protein [36–39]. In contrast, the spectrum obtained with an unstructured Ag pad (Figure 2(c) and blue line in Figure 5) contains only one pronounced band from the buffer solution and does not show any protein vibration modes.

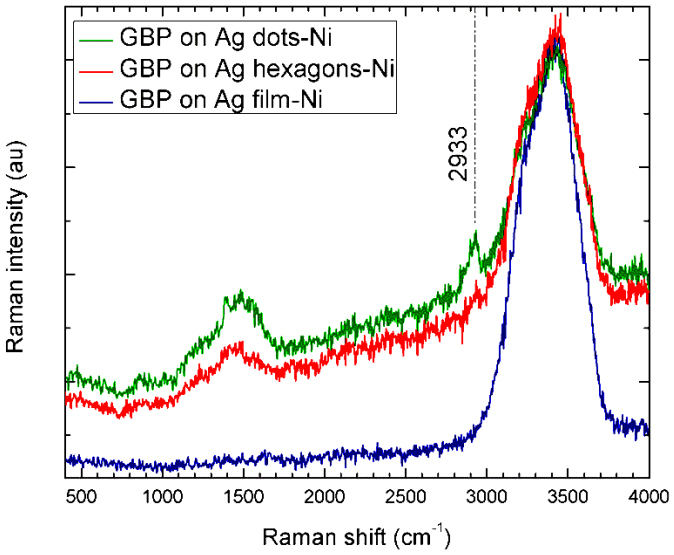


**Figure 5.** SERS spectra for immobilized ligand-free GBP on three different substrates: Ag nano-dots (green), Ag nano-hexagons (red) and Ag pad (blue) [17].

Figure 6 shows SERS spectra for the ligand (D-glucose) bound GBP on the three substrates. In the spectra corresponding to the arrays of Ag nano-dots and nano-hexagons (green and red lines, respectively), three relevant bands can be observed: the broad band at 1550 $cm^{-1}$ characteristic of various bond vibrations in the protein, and two bands at 2850 $cm^{-1}$ and 2910 $cm^{-1}$ corresponding specifically to C–H vibration regimes. The peak at 2850 $cm^{-1}$ is reasonably close to the 2890 $cm^{-1}$ Raman band from D-glucose in buffer solution seen in Figure 4(b). We attribute the peak to C–H vibrations in D-glucose bound to GBP, with the difference in position originating from excitation of different C–H vibration modes out of multiple closely spaced vibration bands that are known to occur in glucose [40–46]. When the SERS spectrum is acquired from an unstructured Ag pad, the bands corresponding to the protein or the ligand are not observed, similar to the case of ligand-free protein.

For verification purposes, we also attempted to obtain spectra from GBP immobilized on Ni-

coated substrates without Ag nanostructures. As one could expect, such attempts did not produce a useful signal, since Ni coatings alone do not generate plasmonic hot-spots for a sufficient enhancement of Raman scattering by immobilized GBP under a 532 nm excitation wavelength.

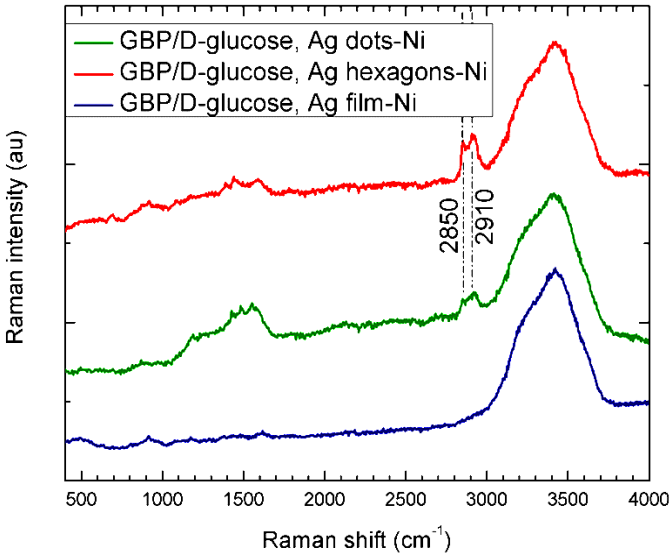


**Figure 6.** SERS spectra for immobilized ligand-bound GBP on three different substrates: Ag nano-dots (green), Ag nano-hexagons (red) and Ag pad (blue) [17].

## 4. Discussion

As Figures 5 and 6 demonstrate, SERS spectra of both ligand-free and ligand-bound GBP are sensitive to the morphology of the substrate. Interestingly, the broad band centered around approximately 1550 $cm^{-1}$ and representative of various vibrations in the protein could be observed on Ag nano-dots (Figure 2(a)) or nano-hexagons (Figure 2(b)) but not on unstructured Ag pads (Figure 2(c)). Since silver structures are known to enhance SERS signal efficiently [4–7], the absence of bands corresponding to the protein in the SERS spectrum from evaporated Ag pads can be attributed to poor binding of GBP to Ag. In contrast, in the other two substrates, Ag nano-dots and nano-hexagons were separated by approximately 25 nm wide gaps with Ni surface exposed, allowing for the histidine-tagged protein binding to nickel [23]. Based on these observations, we hypothesize that GBP binds preferentially to the Ni surface, and therefore most of the SERS signal of the immobilized protein originates from the area around and between the Ag nanostructures.

Figure 7 compares the SERS spectra for immobilized ligand-free and ligand-bound protein for the arrays of Ag nano-dots (Figure 7(a)) and nano-hexagons (Figure 7(b)). For both substrates, the broad band around 1550 $cm^{-1}$ originating from the protein is clearly seen in all spectra. The protein C–H vibration band (2933 $cm^{-1}$) is also well pronounced in the spectra from both ligand-free and ligand-bound GBP on the nano-dots substrate (Figure 7(a)) and is even stronger in that from ligand-bound GBP on the nano-hexagons substrate (Figure 7(b)). However, for ligand-free protein on the nano-hexagons substrate, the protein C–H band is quite weak. The glucose C–H band at 2850 $cm^{-1}$ is marginally discernible in the spectrum of ligand-bound GBP on Ag nano-dots (Figure 7(a)) and well pronounced with nano-hexagons (Figure 7(b)).

Based on the data presented in Figures 5–7, it appears that overall the SERS C–H bands are more pronounced in the spectra from ligand-bound GBP than in the ligand-free one. If one compares the different substrates, the C–H band from ligand-free protein is stronger in SERS spectra obtained with the Ag nano-dots substrate, whereas both the protein and glucose C–H bands from ligand-bound protein are more pronounced with the Ag nano-hexagons substrate. The spectra from evaporated Ag pads do not show any protein or ligand bands, apparently because the GBP does not bind well to Ag, and exposed Ni surface is required for efficient immobilization of the protein. However, such simple considerations do not explain the observed difference in SERS enhancement for ligand-free protein and ligand-bound protein by the two other substrate types.

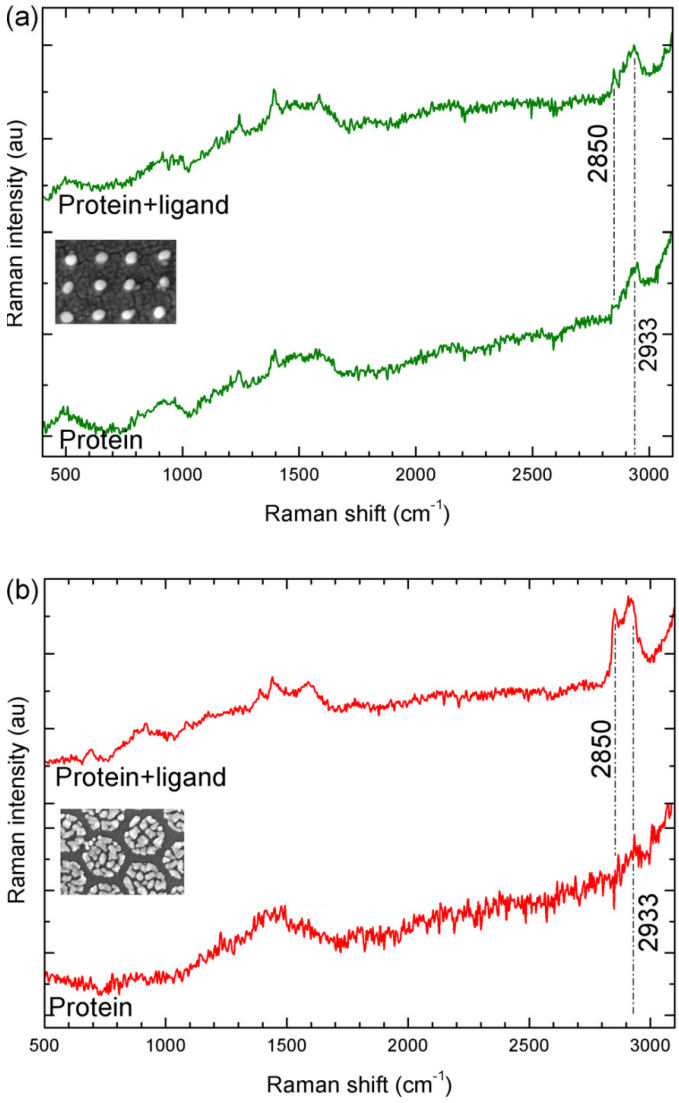


**Figure 7.** SERS spectra for the immobilized ligand-free and ligand-bound GBP for the two nanostructured substrates: (a) array of Ag nano-dots; (b) array of Ag nano-hexagons. In the figures, a vertical offset was applied to the spectra for clearer presentation.

To facilitate interpretations of our observations, we have calculated the scattered electric fields for model SERS substrates as described in Section 2.4. In the model, Ag dots are represented by an

array of nine hemispheres with 10 nm radius and 40 nm pitch as shown in Figures 8(a) and 8(b). The figures depict the simulated distribution of electric field for the array of Ag dots with a 532 nm excitation. The incident wave propagates along the normal to the plane of the substrate, and the direction of the electric field is parallel to the y axis in accordance with the direction of the incident electric field. In Figure 8(a), it can be seen that a high intensity of electric field is generated in the immediate proximity of the borders of the hemispheres.

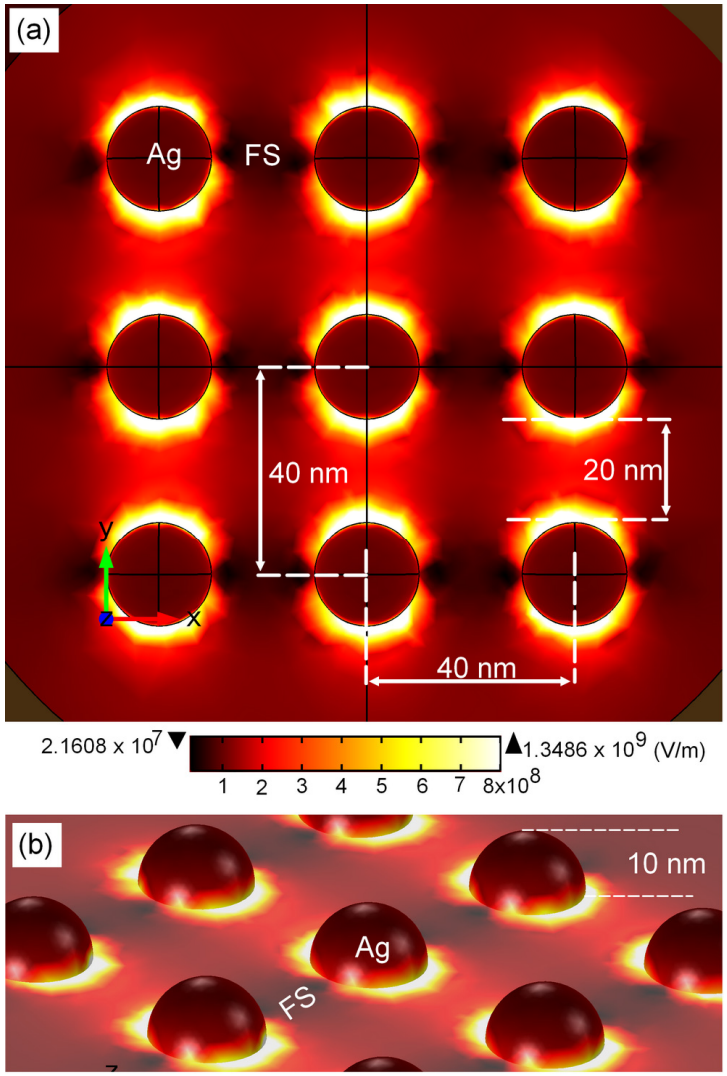


**Figure 8.** Simulated electric field for an array of Ag nano-dots on FS for an excitation wavelength of 532 nm: (a) plan view; (b) 3D view.

To simulate the array of Ag nano-hexagons, we considered the structures with 100 nm long sides composed of smaller closely spaced islands and separated by approximately 20 nm wide gaps matching the morphology of hexagons employed in our experiments (see Figures 2(b) and Figure 9(a)). The thickness of the islands was 10 nm in accordance with that of the evaporated Ag layer, see also Figure 9(b). Figures 9(a) and 9(b) show the predicted electric field for an array of such hexagons. It can be seen that the most significant field enhancement occurs in tiny sub 10-nm gaps between Ag islands of which the nano-hexagons are composed. At some of such "hot spots", the

electric field is significantly stronger than around the hemispherical dots in Figure 8.

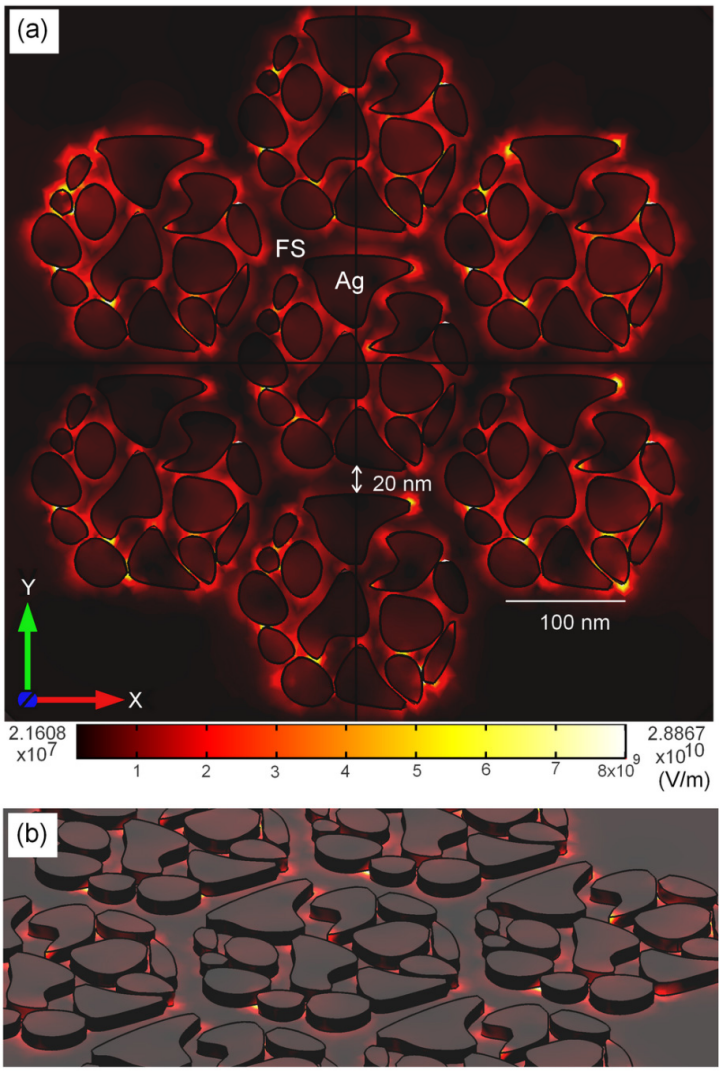


**Figure 9.** Simulated electric field for nano-hexagons composed Ag islands, for an excitation wavelength of 532 nm: (a) plan view; (b) 3D view.

In Figures 10 (a) and (b), the scattered electric field is shown as a function of coordinate y across the brightest "hot spots" for the arrays of nano-dots and nano-hexagons, respectively. In accordance with expectations, it can be seen that the electric field is enhanced preferentially in the proximity of metallic nanostructures. For the array of half-spheres representing Ag nano-dots, a consistent distribution of the field is formed around each dot, with stronger enhancement close to the borders of the dot and a lower level of the field elsewhere (see Figures 8 and Figure 10(a)). For the nano-hexagon structures composed from several smaller islands, a significantly stronger electromagnetic enhancement is observed at several locations in the narrow sub-10 nm gaps between the islands (Figures 9 and Figure 10(b)). However, because of irregular shapes in the islands, these hot spots appear randomly positioned. The strongest hot spots are also relatively few in number. In the wider 20 nm gaps between nano-hexagons, the field tends to be close in magnitude to that in similar gaps between the nano-dots.

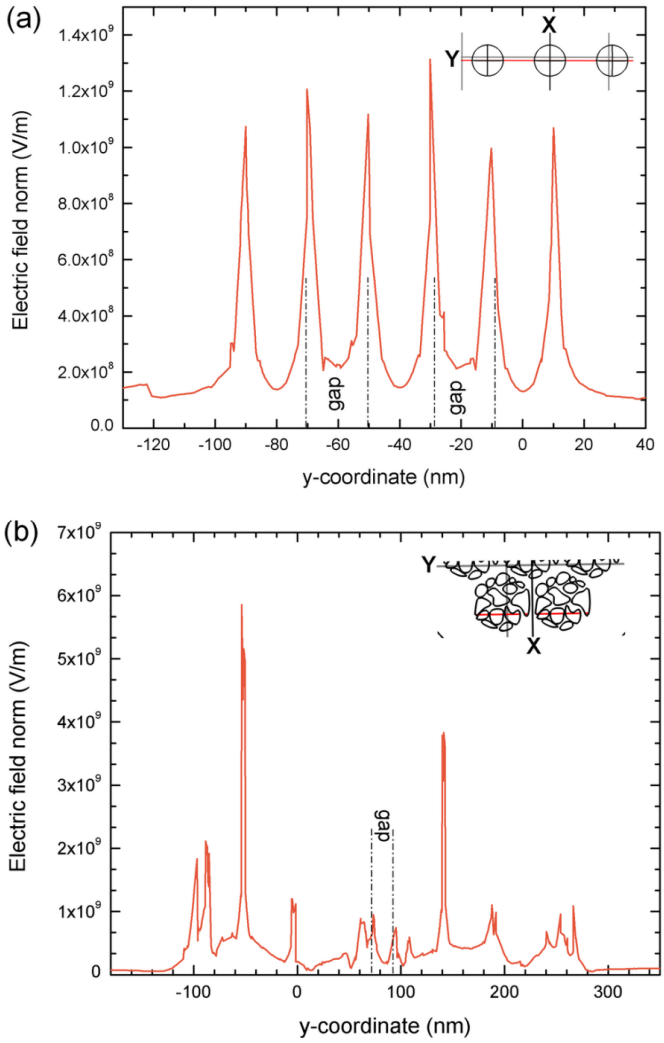


**Figure 10.** Scattered electric field as a function of y-coordinate across hot spots of Ag nanostructures exposed to 532 nm excitation: (a) for dots and (b) for hexagons. The red lines in the insets show the regions where the curves were acquired. The z-coordinate corresponds to 2 nm above the substrate surface.

Note that similar 10-nm gaps can also be found in Ag pads (Figure 3(c)), and they may produce strong hot-spots as well. However, large GBP molecules cannot enter the narrow gaps deep enough to bind to the underlying nickel surface. Without proper binding, any adsorbed GBP molecules are removed during rinsing. The advantage of nano-hexagons is that some of the narrow gaps have exits at the borders, allowing an enhancement in GBPs immobilized outside of the hexagons without their inserting into the gaps.

Our experimental results and numerical predictions suggest that the observed SERS enhancement of C–H vibration bands from ligand-free protein depends on the availability of open Ni surface between the structures where the protein could bind, and also on the scattered electric field in these inter-structure gaps. According to the geometry of our nanostructures, the array of nano-dots offers a relatively larger inter-feature area where the Ni surface is available, and therefore the SERS bands of ligand-free GBP from the nano-dots substrate are more pronounced. This hypothesis may explain a more pronounced 2933 $cm^{-1}$ C–H vibration band observed for the Ag nano-dots substrate

(green line in Figure 5) than for the nano-hexagon substrate (red line in the figure) since the array of nano-dots offers a relatively larger inter-feature area where Ni surface is available for the protein to bind. The case of ligand-bound GBP is more complex. For the family of periplasmic binding proteins to which the GBP belongs, the presence of the ligand in the binding pocket is known to result in a significant change of the protein conformation [21,22]. We hypothesize that in our experiments, immobilized glucose-bound GBP adopts a more compact and less flexible conformation, resulting in increased Raman activity because of an overall better alignment between the plane of polarization of the excitation light and the molecular vibrations. This could produce an increase of the SERS signal from the immobilized GBP molecules. Furthermore, if the gyration radius of GBP decreases upon ligand binding, then some of the ligand-bound protein molecules may be accommodated in narrower inter-island gaps at the borders of nano-hexagons where the electric field is strongest, resulting in the observed enhancement of the SERS signal particularly from the hexagons substrate. Although some of the details require further work to better understand the exact mechanisms involved with the particular analytes and the SERS substrates, overall our results clearly demonstrate the difference of SERS signatures from ligand-free and ligand bound substrate-immobilized GBP, and therefore the potential of SERS to probe protein-ligand molecular recognition.

## 5. Conclusions

We have investigated the influence of SERS substrate morphology on the detected signatures of immobilized ligand-free GBP and ligand-bound GBP complex in solution. In the substrates, a thin Ni layer was used to immobilize a histidine-tagged protein, on top of which plasmonic Ag nanostrucutres were employed to generate SERS hot spots. For this purpose, arrays of Ag nano-dots and nano-hexagons separated by approximately 25 nm gaps were fabricated using electron beam lithography. Unstructured Ag pads on otherwise similar Ni-coated dielectric wafers were also prepared for comparison. Ligand-free and ligand-bound histidine-tagged GBP were immobilized on the substrates, and SERS spectra were acquired while the samples were kept in potassium phosphate buffer solution.

The spectra obtained from nanostructured substrates with Ag nano-dots and nano-hexagons on Ni-coated FS wafers exhibited bands characteristic of the GBP and the ligand (D-glucose), whereas the spectra from Ag pads only showed a band from the buffer solution. We attribute this to selective immobilization of histidine-tagged GBP on the Ni-coated surface in the gaps between Ag nanostructures and to the absence of the analyte bound on the Ag surface.

For nanostructured substrates with Ag nano-dots and nano-hexagons, the SERS signatures of ligand-free GBP and ligand-GBP complex exhibited important differences. The C–H band from ligand-free GBP was more pronounced with the Ag nano-dots substrate, whereas both the GBP and glucose C–H bands from the ligand-protein complex were more pronounced with the Ag nano-hexagons substrate. We hypothesize that the differences may be attributed to a change in the GBP conformation upon binding of D-glucose, resulting in an increase of Raman activity of the analyte and a decrease of its gyration radius.

By employing numerical modeling, we have analyzed the distribution of scattered electric fields for arrays of Ag nano-dots and nano-hexagons. In accordance with expectations, we found that the strongest field enhancement occurs in immediate proximity to the Ag nanostructures. For Ag nano-dots, the distribution of the field was more uniform throughout the array, whereas for nano-hexagons

composed from smaller Ag islands, a significantly stronger electromagnetic enhancement was observed at several random locations in narrow sub 10-nm gaps between the islands. We hypothesize that, due to a change of conformation upon the ligand binding, some of glucose-bound GBP molecules might be accommodated in narrow inter-island gaps at the borders of the nano-hexagons, where their Raman signals were enhanced vigorously.

Overall, our results demonstrate a high potential value of SERS for the characterization of substrate-immobilized proteins and protein-ligand complexes in submonolayer quantities. Binding of D-glucose to the GBP was found to alter the SERS signature, promising future applications of SERS as a powerful method for sensing of small molecules through their recognition by surface-immobilized biopolymers. Both basic studies of molecular recognition, and applications such as detection of small molecules in solution, may benefit of this sensitivity. However, the morphology of plasmonic nanostructures emerges as a major factor determining the capabilities of SERS bio-detection. In the case of relatively large histidine-tagged protein and the Ag/Ni/FS substrate designs that we have explored, the availability and width of gaps between Ag features where the analyte might be accommodated appears to play a key role. This in turn emphasizes the importance of fabrication method employed to prepare SERS substrates. In the present work, positional control achieved through EBL was instrumental to investigate SERS enhancement in the various substrates.

These results indicate that substrate optimization for bio-detection employing proteins as the recognition elements should combine in one comprehensive design: regular and highly-reproducible metallic nano-structure, as achieved in the nano-dots substrate; narrow inter-feature gaps as obtained in the nano-hexagons and Ag pads; and a sufficient inter-feature space to accommodate the protein molecules in their native conformations as reached in the nano-dots and nano-hexagons substrates. Such all-around substrates will facilitate the detection of subtle changes in the conformation and dynamics of biological analytes upon ligand binding.

## Acknowledgments

The authors thank David S. Wishart and Mark T. McDermott for helpful discussions of the work, and the staff of the University of Alberta nanoFAB, NINT Electron Microscopy Facility, and Organic/Inorganic Analytical Lab for technical support. We also gratefully acknowledge Valentyna Semenchenko from D.S. Wishart's research group at the University of Alberta, who kindly provided the glucose binding protein and D-glucose, and Jonathan Mane for his assistance with generating the image of the protein employing VMD version 1.9.1 [47]. The work was supported by the Natural Sciences and Engineering Research Council of Canada, the National Institute for Nanotechnology (NINT) and the University of Alberta.

## Conflict of Interest

The authors are not aware of a conflict of interest to disclosure.

## References

1. Ross AM, Lahann J (2015) Current trends and challenges in biointerfaces science and engineering. *Annu Rev Chem Biomol* 6: 161–186.

2. McKeating KS, Aubé A, Masson JF (2016) Biosensors and nanobiosensors for therapeutic drug and response monitoring. *Analyst* 141: 429–449.
3. Liu Q, Wu Ch, Cai H, et al. (2014) Cell-based biosensors and their application in biomedicine. *Chem Rev* 114: 6423–6461.
4. Ding SY, Yi J, Li JF, et al. (2016) Nanostructure-based plasmon-enhanced Raman spectroscopy for surface analysis of materials. *Nat Rev Mater* 1: 16021.
5. Bonifacio A, Cervo S, Sergo V (2015) Label-free surface-enhanced Ranam spectroscopy of biofluids: fundamental aspects and diagnostics applications. *Anal Bioanal Chem* 407: 8265–8277.
6. He L, Liu Y, Liu J, et al. (2013) Core-shell noble-metal@metal-organic framework nanoparticles with highly selective sensing property. *Angew Chem Int Ed* 52: 3741–3745.
7. Kleinman SL, Frontiera RR, Henry AI, et al. (2013) Creating, characterizing, and controlling chemistry with SERS hot spots. *Phys Chem Chem Phys* 15: 21–36.
8. Jahn M, Patze S, Hidi IJ, et al. (2016) Plasmonic nanostructures for surface enhanced spectroscopic methods. *Analyst* 141: 756–793.
9. Justino CIL, Freitas AC, Pereira R, et al. (2015) Recent developments in recognition elements for chemical sensors and biosensors. *Trac-Trends Anal Chem* 68: 2–17.
10. Luo SC, Sivashanmugan K, Liao JD, et al. (2014) Nanofabricated SERS-active substrates for single-molecule to virus detection in vitro: A review. *Biosens Bioelectron* 61: 232–240.
11. Shiohara A, Wang Y, Liz-Marzan L (2014) Recent approaches toward creation of hot spots for SERS detection. *J Photoch Photobio C* 21: 2–25.
12. Mohammad MA, Muhammad M, Dew SK, et al. (2012) Fundamentals of electron beam exposure and development, In: Stepanova M, Dew SK, *Nanofabrication, Techniques and Principles*, Wien: Springer-Verlag, 11–41.
13. Chen Y (2015) Nanofabrication by electron beam lithography and its applications: A review. *Microelectron Eng* 135: 57–72.
14. Muhammad M, Buswell SC, Dew SK, et al. (2011) Nanopatterning of PMMA on insulating surfaces with various anticharging schemes using 30 keV electron beam lithography. *J Vac Sci Technol B* 29: 06F304.
15. Peters R, Fito T, Gutierrez-Rivera L, et al. (2013) Study of multilayer systems in electron beam lithography. *J Vac Sci Technol B* 31: 06F407.
16. Gutierrez-Rivera L, Peters R, Dew S, et al. (2013) Application of EBL fabricated nanostructured substrates for SERS detection of protein A in aqueous solution. *J Vac Sci Technol B* 31: 06F901.
17. Peters RF, Gutierrez-Rivera L, Dew SK, et al. (2015) Surface enhanced Raman spectroscopy detection of biomolecules using EBL fabricated nanostructured substrates. *J Vis Exp* 97: 52712. Available from: http://www.jove.com/video/52712.
18. Anker JN, Hall WP, Lyandres O, et al. (2008) Biosensing with plasmonic nanosensors. *Nat Mater* 7: 442–453.
19. Bantz KC, Meyer AF, Wittenberg NJ, et al. (2011) Recent progress in SERS biosensing. *Phys Chem* 13: 11551–11567.
20. Sun F, Bai T, Zhang L, et al. (2014) Sensitive and fast detection of fructose in complex media via symmetry breaking and signal amplification using surface-enhanced Raman spectroscopy. *Anal Chem* 86: 2387–2394.
21. Dwyer MA, Hellinga HW (2004) Periplasmic binding proteins: a versatile superfamily for protein engineering. *Curr Opin Struc Biol* 14: 495–504.

22. Benson DE, Conrad DW (2001) Design of bioelectronic interfaces by exploiting hinge-bending motions in proteins. *Science* 293: 1641–1644.
23. Ley C, Holtmann D, Mangold KM, et al. (2011) Immobilization of histidine-tagged proteins on electrodes. *Colloid Surface B* 88: 539–551.
24. Fan M, Andrade FS, Brolo AG (2011) A review on the fabrication of substrates for surface enhanced Raman spectroscopy and their applications in analytical chemistry. *Anal Chim Acta* 693: 7–25.
25. Cuneo MJ, Johnson SJ, Beese LS, et al. (2003) High resolution structure of E. coli glucose/galactose binding protein bound with glucose. *Protein Data Bank* ID 2HPH. Available from: http://www.rcsb.org/pdb/explore.do?structureId=2hph.
26. Recombinant glucose-binding protein was synthesized by Valentyna Semenchenko from D.S. Wishart group at the University of Alberta. Available from: http://www.wishartlab.com.
27. Ko H, Singamaneni S, Tsukruk VV (2008) Nanostructured surfaces and assemblies as SERS media. *Small* 4: 1576–1599.
28. Rycenga M, Camargo P, Li W, et al. (2010) Understanding the SERS effects of single silver nanoparticles and their dimers, one at a time. *J Phys Chem Lett* 1: 696–703.
29. Halas NJ, Lal S, Chang WS, et al. (2011) Plasmons in strongly coupled metallic nanostructures. *Chem Rev* 111: 3913–3961.
30. Iqbal T (2017) Coupling efficiency of surface plasmon polaritons: far- and near-field analyses. *Plasmonics* 12: 215–221.
31. He L, Mao C, Cho S, et al. (2015) Experimental and theoretical photoluminescence studies in nucleic acid assembled gold-upconverting nanoparticle clusters. *Nanoscale* 7: 17254–17260.
32. Khoury CG, Norton SJ, Vo-Dinh T (2010) Investigating the plasmonics of a dipole-excited silver nanoshell: Mie theory versus finite element method. *Nanotechnology* 21: 315203.
33. RF Module of COMSOL Multiphysics. Available from: https://www.comsol.com/rf-module.
34. Johnson PB, Christy RW (1972) Optical constants of the noble metals. *Phys Rev B* 6: 4370–4379.
35. Zampolli M, Tesei A, Jensen F, et al. (2007) A computationally efficient finite element model with perfectly matched layers applied to scattering from axially symmetric objects. *J Acoust Soc Am* 122: 1472–1485.
36. Rygula A, Majzner K, Marzec M, et al. (2013) Raman spectroscopy of proteins: a review. *J Raman Spectrosc* 44: 1061–1076.
37. Barth A, Zscherp C (2002) What vibrations tell us about proteins. *Q Rev Biophys* 35: 369–430.
38. Hunt JH, Guyot-Sionnest P, Shen YR (1987) Observation of C–H stretch vibrations of monolayers of molecules optical sum-frequency generation. *Chem Phys Lett* 133: 189–192.
39. Bright A, Renuga-Devi TS, Gunasekaran S (2010) Spectroscopical vibrational band assignment and qualitative analysis of biomedical compounds with cardiovascular activity. *Int J Chem Tech Res* 2: 379–388.
40. Longhi G, Zerbi G, Paterlini G, et al. (1987) Conformational dependence of CH(CD)-stretching in D-glucose and some deuterated derivatives as revealed by infrared and Raman spectroscopy. *Carbohyd Res* 161: 1–22.
41. Soderholm S, Roos YH, Meinander N, et al. (1999) Raman spectra of fructose and glucose in the amorphous and crystalline state. *J Raman Spectrosc* 30: 1009–1018.
42. Korolevich MV, Zhbankov RG, Sivchik VV (1990) Calculation of absorption band frequencies and intensities in the IR spectrum of α-D-glucose in a cluster. *J Mol Struct* 220: 301–313.

43. Vasko PD, Blackwell J, Koenig JL (1972) Infrared and Raman spectroscopy of carbohydrates. Part II: Normal coordinate analysis of α-D-glucose. *Carbohyd Res* 23: 407–417.
44. Spedding FH, Stamm RF (1942) The Raman spectra of the sugars in the solid state and in solution. I. The Raman spectra of α- and β-d-glucose. *J Chem Phys* 10: 176–183.
45. Mahdad-Benzerdjeb A, Taleb-Mokhtari IN, Sekkal-Rahal M (2007) Normal coordinates analysises of disaccharides constituted by D-glycose, D-galactose and D-fructose units. *Spectrochim Acta A* 68: 284–299.
46. Cael JJ, Gardner KH, Koenig JL, et al. (1975) Infrared and Raman spectroscopy of carbohydrates. Part V. Normal coordinate analysis of cellulose I. *J Chem Phys* 62: 1145–1153.
47. Humphrey W, Dalke A, Schulten K (1996) VMD: visual molecular dynamics. *J Mol Graph* 14: 33–38.


AIMS Press